International Journal of Nanomedicine

Dovepress

open access to scientific and medical research

Open Access Full Text Article

ORIGINAL RESEARCH

A Gambogic Acid-Loaded Delivery System Mediated by Ultrasound-Targeted Microbubble Destruction: A Promising Therapy Method for Malignant Cerebral Glioma

Lei Dong[1,*], Nana Li[1,*], Xixi Wei[2], Yongling Wang[2], Liansheng Chang[3], Hongwei Wu[4], Liujiang Song[5], Kang Guo[6], Yuqiao Chang[1], Yaling Yin[2], Min Pan[7], Yuanyuan Shen[8], Feng Wang[1]

[1]Henan Key Laboratory of Medical Tissue Regeneration, School of Basic Medical Sciences, Xinxiang Medical University, Xinxiang, Henan, 453003, People's Republic of China; [2]Department of Physiology and Pathophysiology, School of Basic Medical Sciences, Xinxiang Medical University, Xinxiang, Henan, 453003, People's Republic of China; [3]Department of Human Anatomy, Histology and Embryology, School of Basic Medical Sciences, Xinxiang Medical University, Xinxiang, Henan, 453003, People's Republic of China; [4]Department of Chemistry, Xinxiang Medical University, Xinxiang, Henan, 453003, People's Republic of China; [5]Department of Ophthalmology, Gene Therapy Center, University of North Carolina at Chapel Hill, Chapel Hill, NC, 27517, USA; [6]Department of Oncology, The Third affiliated Hospital of Xinxiang Medical University, Xinxiang, Henan, 453003, People's Republic of China; [7]Department of Ultrasound, Shenzhen Hospital (Futian) of Guangzhou University of Chinese Medicine, Shenzhen, 518034, People's Republic of China; [8]National-Regional Key Technology Engineering Laboratory for Medical Ultrasound, School of Biomedical Engineering, Health Science Center, Shenzhen University, Shenzhen, 518060, People's Republic of China

*These authors contributed equally to this work

Correspondence: Feng Wang, Henan Key Laboratory of Medical Tissue Regeneration, School of Basic Medical Sciences, Xinxiang Medical University, 601 Jinsui Road, Xinxiang, Henan, 453002, People's Republic of China, Email wfeng100@126.com; Min Pan, Department of Ultrasound, Shenzhen Hospital (Futian) of Guangzhou University of Chinese Medicine, No. 6001 Beihuan Avenue, Shenzhen, 518034, People's Republic of China, Email min.pan@siat.ac.cn

Background: The blood–brain barrier (BBB) inhibits the delivery of macromolecular chemotherapeutic drugs to brain tumors, leading to low utilization rates and toxic side effects to surrounding tissues and organs. Ultrasonic targeted microbubble destruction (UTMD) technology can open the BBB, leading to a new type of drug delivery system with particular utility in glioma.

Purpose: We have developed a new type of drug-loaded microbubble complex based on poly(lactic-co-glycolic acid) (PLGA) that targets gambogic acid (GA) to the area of brain tumors through UTMD.

Methods: GA/PLGA nanoparticles were prepared by the double emulsification method, and cationic microbubbles (CMBs) were prepared by a thin film hydration method. The GA/PLGA-CMB microbubble complex was assembled through electrostatic attractions and was characterized chemically. The anti-glioblastoma effect of GA/PLGA-CMB combined with focused ultrasound (FUS) was evaluated by biochemical and imaging assays in cultured cells and model mice.

Results: GA/PLGA-CMB combined with FUS demonstrated a significant inhibitory effect on glioblastoma cell lines U87 and U251 as compared with controls ($P<0.05$). Tumor access and imaging analyses demonstrated that administration of GA/PLGA-CMBs combined with FUS can open the BBB and target the treatment of glioblastoma in a mouse model, as compared with control groups ($P<0.05$).

Conclusion: The combination of PLGA-CMB with FUS provides an effective and biocompatible drug delivery system, and its application to the delivery of GA in a mouse glioblastoma model was successful.

Keywords: microbubbles, cavitation effect, glioblastoma, focused ultrasound

Introduction

Glioblastoma (GBM), which is the most common intracranial tumor, originates in the glial cells. Current therapies, including surgery, radiation therapy, and chemotherapy, present limited efficacies for treating malignant glioma.[1–3] Standard treatment for newly diagnosed patients includes maximal safe resection followed by radiochemotherapy.[4,5]

Received: 2 November 2021
Accepted: 19 April 2022
Published: 3 May 2022

While several therapies have been employed, the treatment of GBM remains challenging. Even with treatment, the median overall survival for patients diagnosed with GBM is two years.

In recent years, multiple drug delivery platforms based on nanotechnology have been developed, some of which have been used in the clinical treatment of various cancers.[6,7] Applications of nano-drugs include doxorubicin-containing liposomes for sarcoma and breast cancer.[8] Nanoparticles prepared with inorganic materials, such as hydrogen oxide nanoparticles,[9] have also been utilized in the treatment of cancer clinical oncology treatment.

However, the fact that currently available nanoparticles have only limited ability to permeate the blood-brain barrier (BBB) and the blood-tumor barrier (BTB) limits the applicability of this technology to cancer research.[10] Importantly, studies have shown that nanoparticles must have diameters less than 40 nm in order to be likely to penetrate the BBB.[11,12] Thus, targeting across the BBB and ability to enter a tumor is an important factor to be considered in the development of drug-loaded nanoparticles in the treatment of brain tumors, including GBM.[8,12,13]

Gambogic acid (GA) is the main active component of a traditional Chinese medicine called garcinia mandshurica. Because of its demonstrated inhibitory effect on a variety of malignant tumor cells, it has become an important anti-cancer candidate drug.[14] Several in vitro and in vivo studies have shown that GA can inhibit a variety of malignant tumor cells, including lung cancer, liver cancer, leukemia, colorectal cancer, pancreatic cancer and breast cancer cells.[15,16] The anti-tumor effects of GA are manifest through multiple mechanisms, such as inducing apoptosis, inhibiting cell proliferation, preventing tumor angiogenesis and blocking tumor cell invasion and metastasis.[17]

Unfortunately, GA has several characteristics that lead to an increased potential for adverse effects. For example, GA is most often administered intravenously and is thus widely distributed in vivo. In addition, because of its short half-life, relatively high concentrations of GA must be administered. These two factors mean that normal tissues are vulnerable to adverse effects during treatment with GA.[15,18] GA has other disadvantages, such as poor solubility and low bioavailability, and it does not readily pass through the BBB, which limits its application in the treatment of brain tumors. Therefore, it is important to find a drug delivery system in order to optimize the utility of GA in the treatment of GBM.[14–17]

Ultrasound-targeted microbubble destruction (UTMD) is a novel delivery system for drugs and genes that represents a technological revolution in cancer treatment.[19–21] Exposure of tumor cells to ultrasound-activated microbubbles increases the permeability of biological barriers, such as cell membranes and the BBB, and it disrupts the tumor microenvironment directly and mechanically through the effects of heat and oxidative stress.[22] The UTMD system therefore can not only be used as a carrier, but it can also increase the permeability of biological barriers so as to improve the utilization rate and thus the therapeutic effect of chemotherapeutic drugs.[19] Accordingly, the UTMD-mediated drug/gene delivery system has shown great potential in tumor therapy.[23] Recently, multiple studies have shown that UTMD-mediated delivery of drugs can improve the tumor-killing effect, thus reducing the toxicity of chemotherapeutic drugs, lowering the development of drug resistance, and allowing the application of specialized drugs to the treatment of other cancers.

We developed a new drug-loaded microbubble complex that includes GA within a poly(lactic-co-glycolic acid)-based cationic microbubble (GA/PLGA-CMB) (Figure 1). This nanoparticle is designed to be used with a focused ultrasound (FUS) probe, which can be placed with brain stereotaxic instrumentation so that it is focused on the area of a tumor. GA/PLGA-CMBs oscillates violently under the action of FUS with specific parameters, creating a cavitation effect,[24,25] which includes steady-state cavitation and instantaneous cavitation.[26,27] When steady-state cavitation occurs in GA/PLGA-CMBs, we predicted that the permeability of the BBB would increase, allowing the GA/PLGA to enter the tumor tissue.[28,29] In this report, we tested several values of ultrasonic intensity in order to optimize the instantaneous cavitation of the GA/PLGA-CMBs, as the impact caused by cavitation may cause damage to the surrounding tumor cells. In addition, after instantaneous cavitation of GA/PLGA-CMBs, we predicted that the GA/PLGA cargo would be uniformly released into the tumor area. Thus, in this report, we present the development and assessment of a new drug-loaded PLGA-CMB microbubble complex, which can target and release drugs under the guidance of ultrasound. This endeavor promises to reduce systemic side effects of chemotherapeutic drugs, improve the utilization rate, prolong the action time, and provide new strategic directions for the treatment of malignancies of the brain.

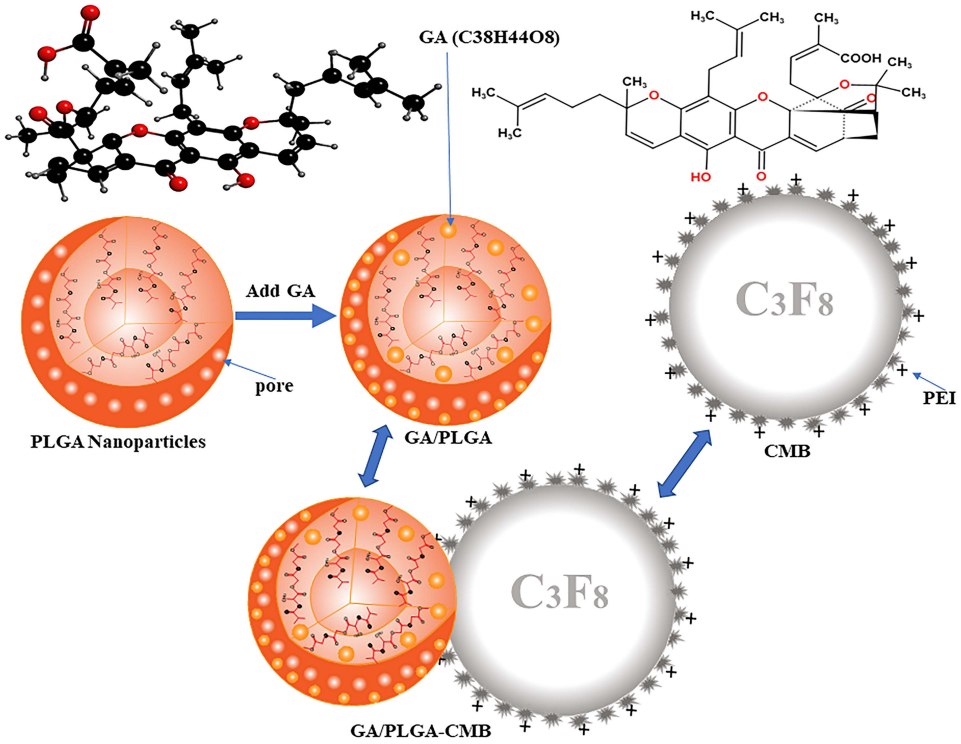

Figure 1 Pattern diagram of GA/PLGA-CMB. The positively charged CMB is combined with the negatively charged GA/PLGA to form a GA/PLGA-CMB microbubble complex.

Materials and Methods

Materials

U87, U251 and bEnd3 cells were purchased from the Chinese Academy of Sciences (Shanghai, China). LV-LUC-GFP-PURO lentivirus was synthesized by Shanghai Hengyuan Biotechnology Co., Ltd (Shanghai, China). GA, PLGA, distearoylphosphatidylcholine (DSPC), 1,2-distearoyl-sn-glycero-3-phosphoethanolamine (DSPE)-PEG2000, and polyethyleneimine (PEI) were purchased from Avanti Polar Lipids (Beijing, China). D-Luciferin potassium salt was purchased from Cayman Chemicals (Ann Arbor, MI, USA). Antibodies against the marker of proliferation Ki-67 and proliferating cell nuclear antigen (PCNA) were purchased from Abcam (Cambridge, MA). Anti-TUNEL antibodies (ab179454) and a TUNEL Assay Kit (ab66110) were from Abcam (Cambridge, MA). Cell viability assays were performed using the Cell Counting Kit-8 (CCK-8, Abcam, Cambridge, UK) assay as per the manufacturer's instructions. A YF488-Annexin V/PI apoptosis detection kit, and Hoechst 33,342 were obtained from US Everbright (San Francisco, CA, USA).

A high-speed refrigerated centrifuge (Hunan Changsha Xiangyi Centrifuge Instrument Co., Ltd, Beijing, China), a Zetasizer Nano ZS 90 (Malvern Instruments, Ltd., Malvern, U.K.), a flow cytometer (Millenia Biotech, Goldbach, Germany), a multi-detection microplate reader (Bio Tek, USA), and stereotaxic instruments (SR-6, Scientific Instrument Lab., Tokyo, Japan) were used. The small animal living imaging system (Lumina LT, PerkinElmer, Inc.) was used for in vivo imaging.

Synthesis of PLGA-CMBs

PLGA and DSPC were dissolved at a mass ratio of 20:1 in 1 to 3 mL dichloromethane. The following ultrasonic parameters were used: power 900 W, power ratio 60%, ultrasonic on time 3 s and off time 3 s, and working cycle 2 min. After 5 mL 4% polyvinyl alcohol was added, the suspension was homogenized for 5 min. Double distilled water (10 mL) was added to the homogenized liquid, and the mixture was stirred for 2 to 3 h. After centrifugation at 4500 rpm for 3

min, the supernatant was discarded, 1 mL double distilled water was added, and the sample was incubated overnight at −80 °C. After freeze-drying for 48 h, PLGA nanobubbles (NBs) were obtained and stored at −20 °C.

A cationic microbubble solution was prepared with DSPC, PEG-2000, PEI and stearic acid as the main components. After air was removed with a vacuum, the cationic microbubble was filled with inert gas (C_3F_8), and the cationic microbubble (CMB) suspension was obtained after shaking for 45s. Aliquots of 100 μL CMB suspension were mixed with 80 μg PLGA NBs, resulting in a PLGA-CMB suspension. Defined amounts of GA were added to the PLGA-CMB raw material to obtain CA/PLGA-CMBs.

Characterization of GA/PLGA-CMBs

The drug loading and entrapment efficiency were calculated by spectrophotometry. The drug loading and entrapment efficiency of GA/PLGA dissolved in DMSO were then calculated. Drug loading was calculated as $LE(\%) = W_e/W_m \times 100\%$, where LE represents drug loading, W_e represents the amount of drug encapsulated in the lipid and W_m represents the total weight of GA/PLGA NBs. Entrapment efficiency was calculated as $EN\% = (1 - C_f/C_t) \times 100$, where EN represents the drug entrapment efficiency as a percentage, C_f is the amount of free drug and C_t is the total amount of drug (free and entrapped). The particle size and potential distribution of GA/PLGA-CMBs were detected by a Malvern particle size analyzer, scanning electron microscopy and transmission electron microscopy.

Physiological Stability of GA/PLGA-CMBs

The GA/PLGA-CMBs showed a good physiological stability. B-mode scan ultrasonography was performed using a Sonix SP High Performance B-mode System (Ultrasonix, Richmond, BC, Canada). The age of BALB/c mice is 6–7 weeks. Each mouse was injected with 100 μL GA/PLGA-CMBs suspension via tail vein. Ultrasound imaging experiments were carried out at 0–40 min. The liver US image in comparative mode was recorded. Further analysis was performed using a high frequency US scanning high-resolution B-mode ultrasonography system. High-resolution B-mode ultrasonography of the right liver was performed with a linear 8 MHz frequency.

Cell Culture

Dulbecco's modified Eagle's medium containing 10% fetal bovine serum and 1% penicillin and streptomycin was used for culturing U87 and U251 cells. Cells were cultured in an incubator at 37 °C and 5% CO_2. Cells were passaged with 0.25% trypsin when confluence reached 80 to 90% at the logarithmic growth phase and were diluted to 1×10^5 cells/mL. Cells were cryopreserved in a solution containing 10% DMSO. Drugs were dissolved in a solvent containing phosphate-buffered saline (PBS) with DMSO (5%) and Tween-80. The concentration of drug was adjusted so that animals were administered 1.5 μmol/L.

Measurements of Drug-Release Behavior

Aliquots (100 μL) of a suspension of GA/PLGA-CMBs were placed in wells of a 96-well plate. The samples were subjected to ultrasound under the following conditions: frequency 949 KHz, 10,000 cycles, 5% duty cycle, 1 s pulse time and 60s action time. The sound pressure intensity was increased from 0 to 0.88 MPa, and the concentration of GA/PLGA-CMBs in suspension at each sound pressure intensity interval was detected by enzyme labeling and spectrophotometry at $\lambda = 500$ nm.

Using the same ultrasonic parameters as above, the viability of U251 cells treated with different sound pressure intensities was detected via CCK-8 assays. Then, U251 cells were incubated with different concentrations of GA for 24 hours, and the cell viability of U251 cells in each group was detected via CCK-8 assays. The GA concentrations of all treatment groups in Figures 2–4 were consistent. The concentration was 1.5 μmol/L.

CCK-8 Assays for Cell Viability

Wells of a 96-well plate were seeded with 100 μL of a 5×10^4 cells/mL suspension, and the plates were then incubated at 37 °C and 5% CO_2 for 24 h in serum-free medium. Then, 10 μL of CCK-8 solution was added to each well. The absorbance at 450 nm was measured 1 h later. Cell viability was determined with the following equation: viability rate $= ((A_s - A_b)/(A_c - A_b)) \times 100$, where

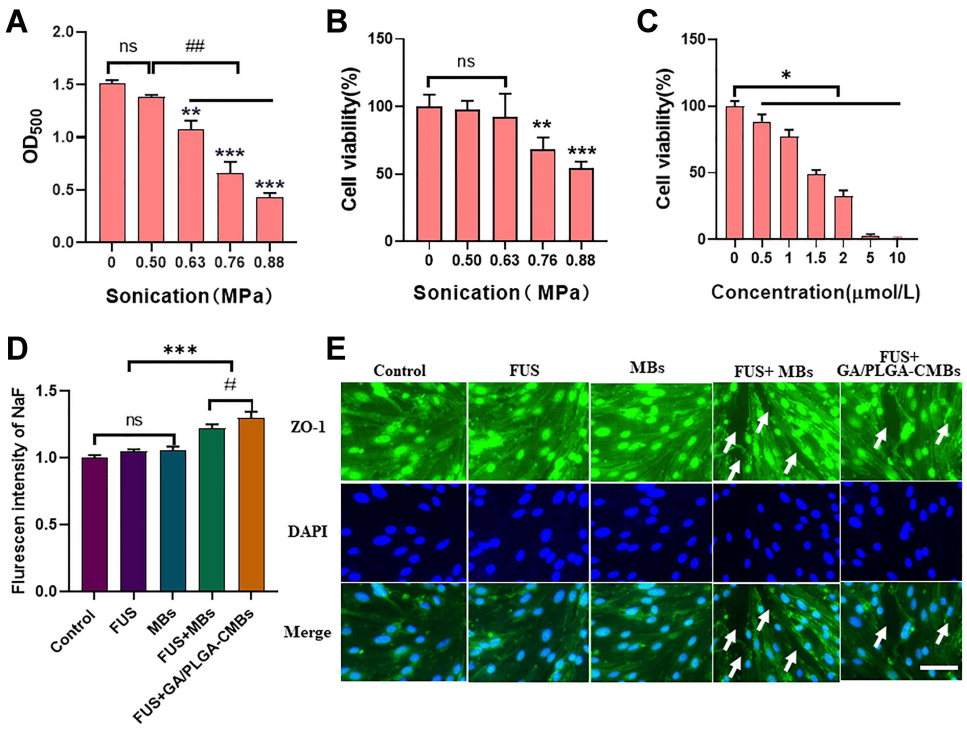

Figure 2 Ultrasound controlled drug release in vitro. (**A**) When the ultrasonic intensity is 0.63–0.88Mpa, GA/PLGA-CMBs can have "cavitation effect" (**p<0.01, ***p<0.001 versus control group, ##p<0.01 versus each other group). (**B**) The activity of U251 cells decreased significantly when the ultrasound intensity was 0.76–0.88 Mpa (**p<0.01, ***p<0.001 versus"0"Mpa group). (**C**) After coincubation of U251 cells with 1.5 μmol/L GA for 24 h, The cell viability of U251 cells was 48.71 ±2.84% (*p<0.05 versus "0"μmol/L group). (**D**) Different treatment groups correspond to the NaF fluorescence signal values in the liquid under the Transwell chamber (***p<0.001, #p<0.05 versus each other group). (**E**) The BBB model in vitro was constructed by bEend3 cells. The Zo-1 antibody was labeled with green immunofluorescence. The nucleus was labeled with DAPI, and the white arrow was marked as the open part of tight junction. Ruler: Bar=50 μm.

A_s was the absorbance of the experimental well including medium, CCK-8 reagent and GA, A_c was the absorbance of the control well without GA and A_b was the absorbance of the blank well without cells or CCK-8 reagent.

Detection of Apoptosis

In order to detect apoptosis by flow cytometry, cells growing in suspension were collected by centrifugation at 500*g* for 5 min, and adherent cells were collected by trypsin digestion without EDTA. Cells were washed with 10 mL PBS and collected by scraping in 5 mL PBS followed by centrifugation at 2000 RPM for 5 min at 4 °C. Then, 300 μL of binding buffer and 195 μL Annexin V-FITC binding buffer were added, followed by incubation with 5 μL annexin V-FITC and 10 μL propidium iodide (PI) for 20 min in the dark. Dual parameter dot plots combining signal from annexin V-FITC and PI revealed living cells in the lower-left quadrant (annexin V−/PI−), early apoptotic cells in the lower-right quadrant (annexin-V+/PI−), late apoptotic cells in the upper-right quadrant (annexin V−/PI+), and necrotic cells in the upper-left quadrant (annexin-V+/PI+).

Apoptosis was also quantified using a microscopy-based kit. Double staining of U87 cells with AlexaFluor 488-annexin V and PI enabled the discrimination of live (AlexaFluor 488-/PI-), early apoptotic (AlexaFluor 488+/PI-), late apoptotic (AlexaFluor 488+/PI+), or necrotic (Alexa Fluor 488-/PI+) cells. Cell nuclei were counterstained with DAPI, and fluorescence images were acquired using a fluorescence microscope (DMI3000B, Leica, Germany). Fluorescent signal was quantified by ImageJ software.

Animals and Tumor Models

Female nude BALB/c mice, aged 6 to 8 weeks, were purchased from Beijing HFK Bioscience (Beijing). They were raised in a specific pathogen-free (SPF) animal room at a constant temperature (25 °C). All animal procedures were reviewed and approved by the Institutional Animal Care and Use Committee at Xinxiang Medical University and are in

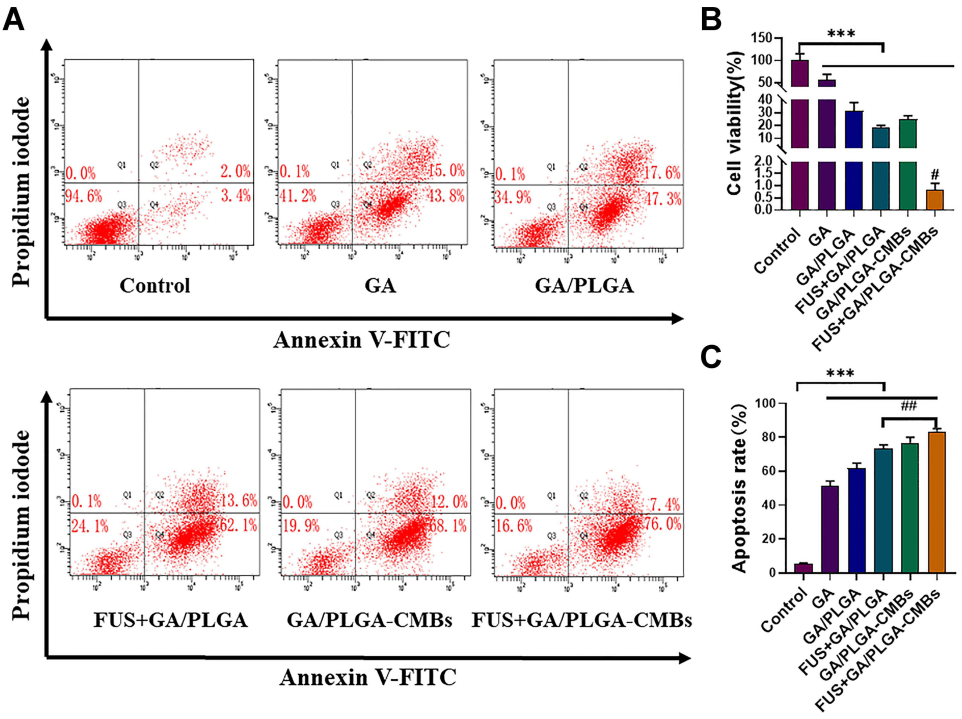

Figure 3 To evaluate the inhibitory effect of FUS combined with GA/PLGA-CMBs on U251 cells. (**A**) Different treatments of U251 cells correspond to the results of flow cytometry. (**B**) After 24 hours of different treatments, the viability of U251 cells in each group was detected by CCK-8. The cell viability of U251 cells in FUS+GA/PLGA-CMBs group was 0.81 ± 0.26% (***p<0.001 versus control group, #p<0.05 versus other groups). (**C**) After 24 hours of different treatments, the apoptosis rate of U251 in each group was detected by flow cytometry. The apoptosis rate of U251 cells in FUS+GA/PLGA-CMBs group was 76.73 ± 2.70% (***p<0.001 versus control group, ##p<0.01 versus each other group).

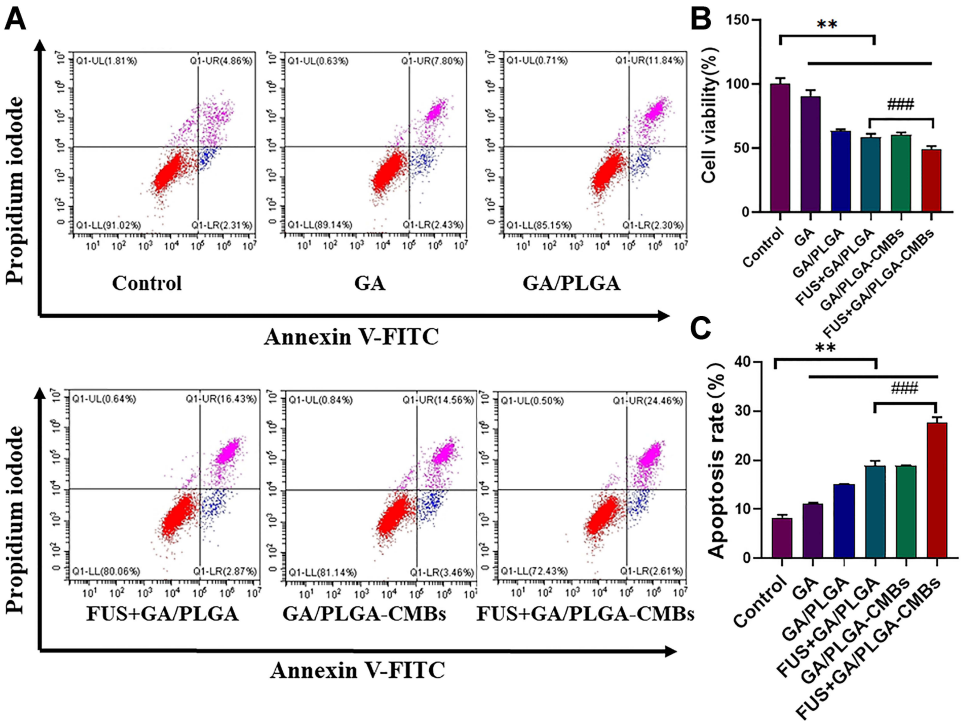

Figure 4 To evaluate the inhibitory effect of FUS combined with GA/PLGA-CMBs on U87 cells. (**A**) Different treatments of U87 cells correspond to the results of flow cytometry. (**B**) After 24 hours of different treatments, the viability of U87 cells in each group was detected by CCK-8. The cell viability of U87 cells in FUS+GA/PLGA-CMBs group was 49.34±1.95% (**p<0.01 versus control group, ###p<0.001 versus each other group). (**C**) After 24 hours of different treatments, the apoptosis rate of U251 in each group was detected by flow cytometry. The apoptosis rate of U87 cells in FUS+GA/PLGA-CMBs group was 27.68±0.89% (**p<0.01 versus control group, ###p<0.001 versus each other group).

accordance with the Guide for the Care and Use of Laboratory Animals of Chinese Academy of Sciences. Ethical review approval number: XYLL—2020516-6.

Mice were anesthetized with 4% isoflurane/O_2 gas, and anesthesia was maintained with 1.5% isoflurane/O_2 gas. U87-Luc cells carrying luciferase (Luc) gene fragments were implanted in order to generate the mouse glioma model. According to the mouse brain atlas, the anterior fontanelle was coordinate zero, and 2.5 μL of a U87-Luc cell suspension in PBS with a cell density of 2×10^5 cells/mL was injected at the coordinate (1.0 mm, 1.5 mm, 2.0 mm). The injection time was 5 min, and the needle was retained for 10 min. Penicillin (10,000 U/day) was injected intramuscularly every day for 1 week following surgery.

Construction of the in vitro BBB Model

Cells of the mouse brain microvascular endothelial cell line bEend3 were inoculated on a Transwell membrane. After 5 days of routine culture, the in vitro BBB model was established. High glucose medium (500 μL) was added to the upper and lower chambers of the Transwell apparatus, and 500 μL of NaF (10 μg/mL) was added to the upper chamber.

The BBB model was treated with 5 different treatments: untreated (control), ultrasound-only (FUS), empty phospholipid microbubbles (MB), ultrasound combined with empty phospholipid microbubbles (FUS+MB) and ultrasound combined with drug-loaded microbubble complex (FUS+GA/PLGA-CMB). The system was treated with ultrasound following the parameters noted above, and the sound pressure intensity was 0.63 MPa. Cells were stained with an anti-Zo-1 antibody and a secondary antibody that was indicated by green fluorescence, and DAPI-labeled nuclei were blue as observed by fluorescence microscopy. The fluorescence signal value of NaF in the lower chamber was detected by an enzyme labeling instrument.

In vivo Assays of BBB Opening

The experiment was divided into three groups: a group treated only with ultrasound (FUS), a group treated with ultrasound and GA/PLGA microbubbles (FUS+GA/PLGA) and a group treated with ultrasound combined with the drug-loaded microbubble complex (FUS+GA/PLGA-CMB). For treatment, 50 μL of a GA/PLGA or GA/PLGA-CMB suspension was injected into the tail vein of each mouse. After 1 min, the sound pressure intensity was adjusted to 0.50, 0.63, 0.76, 0.88 or 1.01 MPa for 30s. After the treatment of FUS combined with GA/PLGA-CMBs, the corresponding brain tissue was perfused and processed under different sound pressure intensities, embedded in paraffin, stained with hematoxylin and eosin, and stained with DAPI (nuclei) and TUNEL (apoptotic cells). Hematoxylin and eosin (H&E) staining was performed according to a standard H&E protocol. The apoptosis rate, as determined by TUNEL labeling, was assessed with ImageJ software.

In vivo Imaging

Anesthesia of mice was induced with continuous application of 1.5% isoflurane. Each mouse was injected intraperitoneally with 100 μL of a solution of D-fluorescein potassium salt (Alameda, CA, USA; 15 mg/mL in normal saline). After 15 min, the fluorescence signal was detected with a live animal imaging system (IVIS) (Lumina LT; PerkinElmer, Inc.).

Evaluation of Anti-Tumor Effects

Brain glioma model mice were treated on the 10th day after successful establishment of the glioma model. The treatment occurred once every 2 days for a total of 3 treatments. The mice in each group were imaged by IVIS on days 10, 17 and 24 after successful establishment of the glioma model. On day 17, the brains were perfused, and the tumor tissues were sectioned in paraffin. An anti-PCNA antibody and an anti-Ki-67 antibody were used to detect tumor proliferation. TUNEL assays were performed using a TUNEL Apoptosis Detection Kit (Keygentech, China) for the detection of apoptotic tumor cells in the paraffin-embedded tumor tissue. At day 37 following establishment of the model, the brains were perfused to observe the appearance of the tumor tissue, and the tumor volumes were measured. The number of mice surviving in each group on day 60 was recorded.

Statistical Analysis

Data were analyzed using SPSS 22.0 statistical software and presented as the mean ± SD. The one-way ANOVA test was applied for evaluating possible statistical differences among three or more groups of data. $P < 0.05$ was considered statistically significant (In each figure, statistical significance is indicated with the following symbols: *P < 0.05, **P < 0.01, ***P < 0.001, #P < 0.05, ##P < 0.01, ###P < 0.001, nsP > 0.05).

Results

Synthesis and Characterization of GA/PLGA-CMB

The results of scanning electron microscopy (SEM) and tunneling electron microscopy (TEM) analyses showed that the GA/PLGA was spherical, the surface contained both drug molecules and pores, and the particle sizes were dispersed uniformly (Figure 5A and B). CMBs were manifest as spherical and hollow structures under TEM (Figure 5C). The GA/PLGA-CMB complexes were confirmed to be composed of both CMBs and GA/PLGA (Figure 5D) according to TEM images.

The entrapment efficiency and drug loading was quantified by adding varying amounts of GA nanoparticles to a constant mass (50 mg) of PLGA. Here, the entrapment efficiency and drug loading of GA/PLGA prepared by adding GA in a ratio of 4 mg GA to 50 mg PLGA were 83.04 ± 7.51% and 6.64 ± 0.60%, respectively (Figure 5E and F). Malvern particle size analyses showed that the average particle size distribution of the GA/PLGA-CMBs was 951.37 ± 110.32 nm,

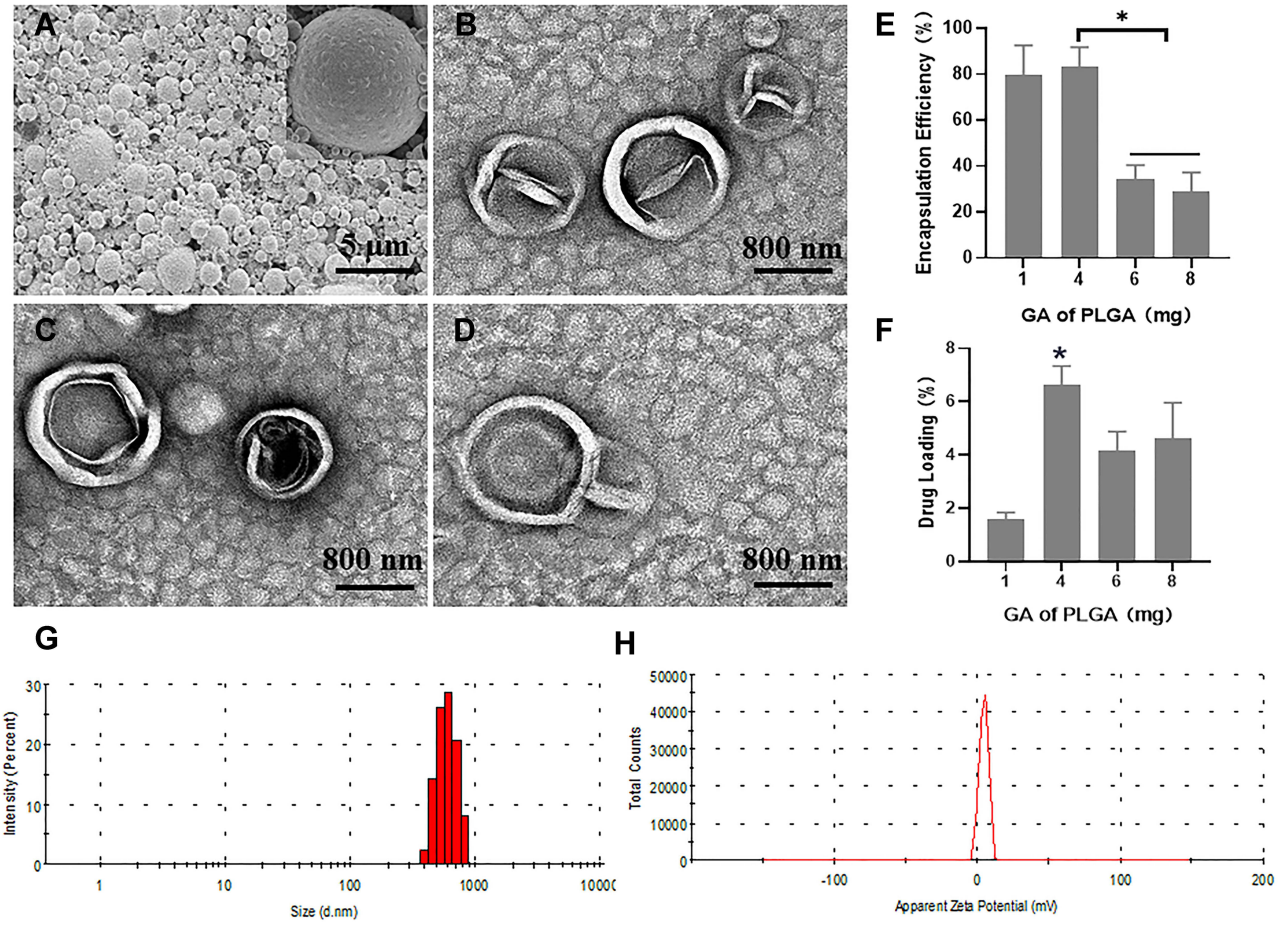

Figure 5 Characterizations of GA/PLGA-CMBs. (**A**) GA/PLGA was spherical and uniformly dispersed under scanning electron microscope (SEM). (**B**) GA/PLGA was spherical and wrinkled under transmission electron microscope (TEM). (**C**) CMBs showed spherical and hollow structure under TEM. (**D**) GA/PLGA-CMBs is composed of CMBs and GA/PLGA under transmission electron microscope. (**E** and **F**) Every 50 mg PLGA, 4 mg GA is added to prepare GA/PLGA. The entrapment efficiency of GA/PLGA was 83.04% ± 7.51% (*p<0.05 versus each other group). The drug loading of GA/PLGA was 6.64 ± 0.60% (*P <0.05 versus other three groups). (**G** and **H**) The particle size distribution of GA/PLGA-CMBs is 951.37 ± 110.32 nm.The potential distribution of GA/PLGA-CMBs was 5.30 ± 0.49 mV.

and the potential distribution was 5.30 ± 0.49 mV (Figure 5G and H). The distribution was shown to be normal. The results of physiological stability test showed that GA/PLGA-CMBs could persist around 30 min in vivo (Figure 6).

Drug Loading and Release

To measure the ability of the particles to release drug upon application of ultrasound, FUS was applied under conditions noted in Materials and Methods, and the quantity of drug released was determined by measuring the spectroscopic absorbance of the supernatant at 500 nm. The concentration of drug released upon application of a sound pressure of 0.63 MPa (OD_{500} = 1.07 ± 0.07) was significantly different from that when the sound pressure was zero (OD_{500} = 1.51 ± 0.03) (P < 0.01, Figure 2A).

The biological effects of this sound application were also tested. When the sound pressure intensity was 0.63 MPa, FUS had no effect on the viability of U251 cells, as detected by CCK-8 assays. The U251 cell viability was 68.17 ± 7.70% when the sound pressure intensity was 0.76 MPa, and the U251 cell viability was 54.59 ± 4.01% when the sound pressure intensity was 0.88 Mpa. The difference in cell viability following treatment with 0.76 MPa was significantly higher than that following treatment with 0.88 MPa FUS (P < 0.01, Figure 2B).

After U251 cells were incubated with free GA at 1.5 μmol/L for 24 h, the cell viability was 48.71 ± 2.84%, which was significantly lower than the viability of cells treated with vehicle for 24 h, which was defined as 100% (p < 0.05, Figure 2C).

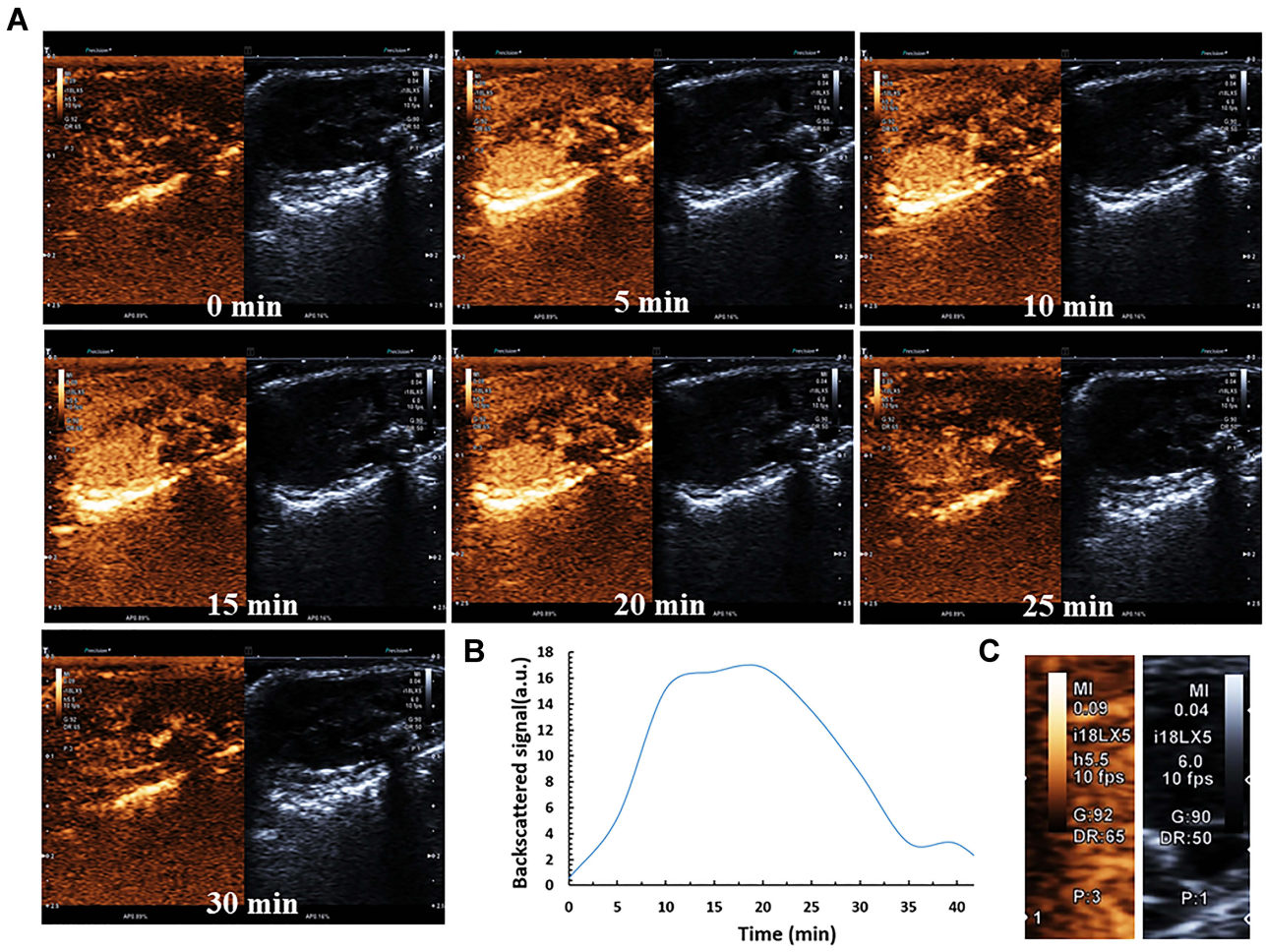

Figure 6 The stability of the GA/PLGA-CMBs under physiological condition. (**A–C**) each mouse was injected with 100 μL GA/PLGA-CMBs suspension via tail vein. In B mode and enhanced contrast mode, liver imaging was detected before and after injection of suspension. The in vivo imaging duration of GA/PLGA-CMBs was 30 min. n=3.

Application of FUS combined with GA/PLGA-CMBs was found to open the model BBB (see, especially, the white arrow in Figure 2D). After opening the model BBB, NaF was able to infiltrate from the upper chamber of the model apparatus into the liquid in the lower chamber. The opening of the BBB was demonstrated by an increase of the NaF signal to 1.30 ± 0.04% in the lower chamber solution, which was significantly higher than the signal in the control system ($p < 0.001$, Figure 2D and E).

Inhibition of Growth of Brain Glioma Cell Lines

U251 cells were treated with FUS and GA/PLGA-CMBs for 24 h. The final drug concentration was 1.5 μmol/L relative to GA, the sound pressure intensity was 0.63 MPa, the action time was 30s, and other FUS parameters were as noted in Materials and Methods. Following the treatment, the rate of apoptosis was detected by flow cytometry. The rate of apoptosis of cells treated with FUS and GA/PLGA was 76.73 ± 2.70%, and the rate of apoptosis of cells treated with FUS and GA/PLGA-CMB was 83.43 ± 1.43%. As shown in Figure 3A and C, the difference in the rate of apoptosis between these two treatment groups was significant ($p < 0.001$).

The viability of U251 cells post-treatment was detected by CCK-8 (Figure 3B). The viability of cells treated with FUS and GA/PLGA-CMB was 0.81 ± 0.26%, which was significantly different from the viability of control cells 100 ± 13.62% ($p < 0.001$).

We performed the same test with another GBM cell line, U87, and the results were similar to those found for U251. Here, the rate of apoptosis of U87 cells treated with FUS and GA/PLGA-CMB (27.68 ± 0.89%) was significantly higher than that of apoptosis of cells treated with FUS and GA/PLGA (18.9 ± 0.78%; $p < 0.01$; Figure 4A and C). The viability of U87 cells treated with FUS and GA/PLGA-CMB was 49.34 ± 1.95% and was significantly different from that of the control group ($p < 0.01$; Figure 4B).

After U87 cells were cultured for 24 h under various treatments, rates of apoptosis were detected using a YF488-Annexin V/PI apoptosis detection kit (Figure 7A). Early apoptotic cells were labeled with YF488, and late apoptotic cells

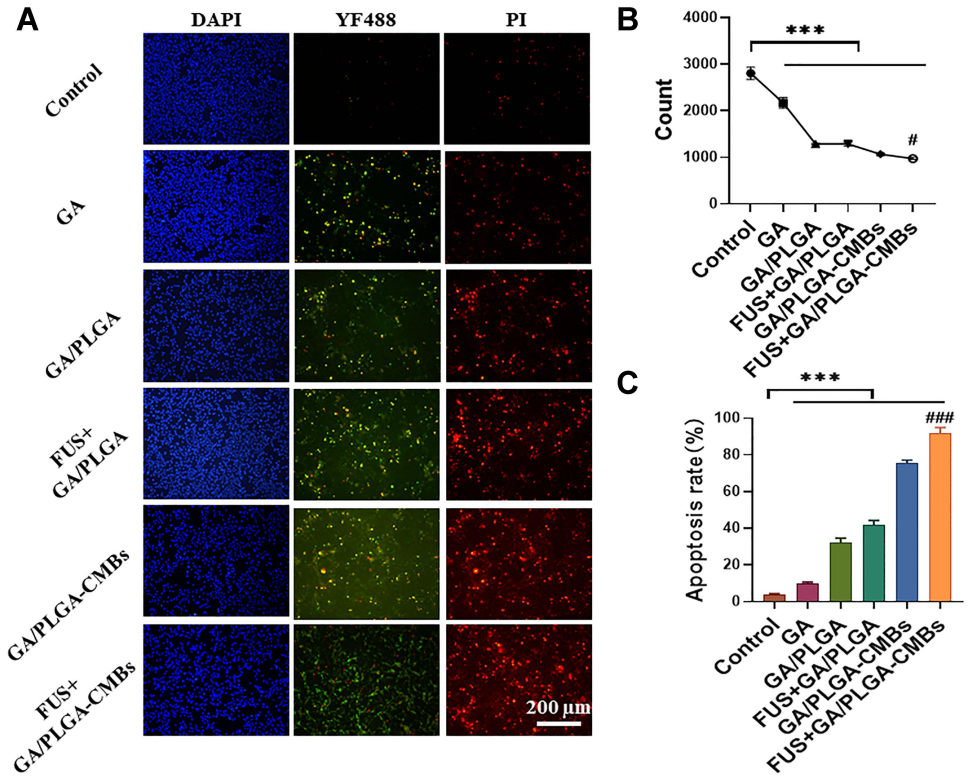

Figure 7 FUS+GA/PLGA-CMBs treatment inhibits the growth of U87 glioma cells. (**A**–**C**) Apoptosis was also evaluated by YF488-Annexin V/PI apoptosis detection kit, after the U87 cells of different treatment were incubated for 24 h. Values were presented as mean ± SD, n= 5.*** P <0.001, between groups. Compared with the Control group, Values were presented as mean ± SD, n= 5. # P <0.05. ### P <0.001.

were labeled with PI. The nuclei of cells in each group were labeled with DAPI, and the cells in each group were counted using ImageJ. The results showed that compared with other groups, the number of U87 cells in the group treated with FUS and GA/PLGA-CMB was the lowest ($P < 0.001$; Figure 7B). The results also demonstrated that apoptosis and necrosis occurred in all of the groups of U87 cells. The apoptotic rate of U87 cells treated with FUS and GA/PLGA-CMB was the highest, and it was significantly higher than that of other groups ($P < 0.001$; Figure 7C). In addition, this experiment demonstrated that FUS combined with GA/PLGA-CMB induced the apoptosis of U87 cells only under certain ultrasound parameters (Figure 7). These results suggest that the sound pore effect mediated by GA/PLGA-CMB under the action of FUS increased the permeability of the U87 cell membrane, promoted the entry of GA/PLGA into U87 cells, stimulated the release of GA, and increased the apoptotic rate of U87 cells.

Opening of the BBB in vivo

We used a mouse model to further explore the opening of the BBB in vivo. The permeability of the blood-brain barrier was evaluated using Evans blue dye (EB, Sigma Co. USA). The results of permeability studies show that FUS combined with GA/PLGA-CMBs enhanced the opening of the BBB when the ultrasonic intensity was between 0.63 and 1.01 MPa. FUS alone or FUS with GA/PLGA did not open the BBB (Figure 8). The brain tissues of mice treated with different ultrasound intensities were embedded in paraffin and stained with H&E (Figure 9A). Microscopic analyses of these tissues showed that when the ultrasound intensity was between 0.69 and 0.88 MPa, the erythrocyte extravasation became obvious (Figure 9B). The relative amount of erythrocyte exudation (86.67 ± 9.53) was significantly higher than that in tissues treated with an ultrasound intensity of zero MPa (7 ± 1.63; $p < 0.05$).

We also labeled apoptotic cells using a TUNEL kit and labeled nuclei with DAPI. Quantification of the rate of apoptosis demonstrated that the rate of apoptosis was relatively high when the ultrasound intensity was between 0.69 and 0.88 MPa. When the ultrasound intensity was 0.88 MPa, the rate of apoptosis was $79.03 \pm 5.12\%$ and was significantly higher than that in tissues treated with an ultrasound intensity of zero MPa ($16.03 \pm 2.41\%$; $p < 0.05$) (Figure 9C).

Evaluation of the Anti-Tumor Effect

IVIS was used to detect the growth of tumors in mice treated under various conditions. The treatment began on the day 10 after the establishment of the model and was performed once every 2 days, for a total of 3 treatments. The luciferase

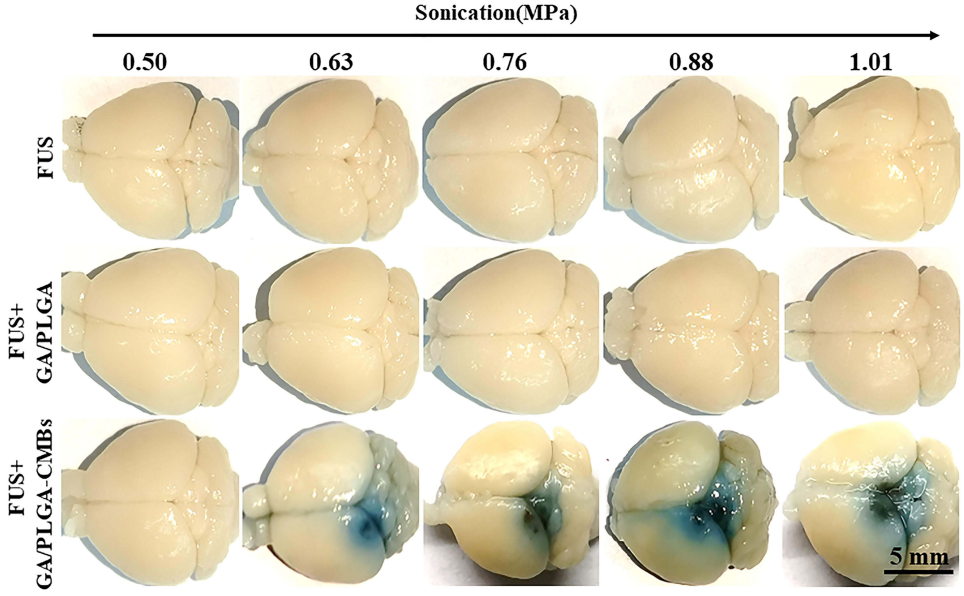

Figure 8 The blood-brain barrier (BBB) was opened by FUS combined with GA/PLGA-CMBs. 100 μL GA/PLGA or GA/PLGA-CMBs suspension was injected into the tail vein of mice. After 1min, the FUS with sound pressure intensity of 0.50,0.63,0.76,0.88 or 1.01Mpa worked for 30 seconds. When the ultrasonic intensity is 0.63–1.01 Mpa, FUS combined with GA/PLGA-CMBs can open BBB. FUS alone or FUS combined with GA/PLGA cannot open BBB. n=3.

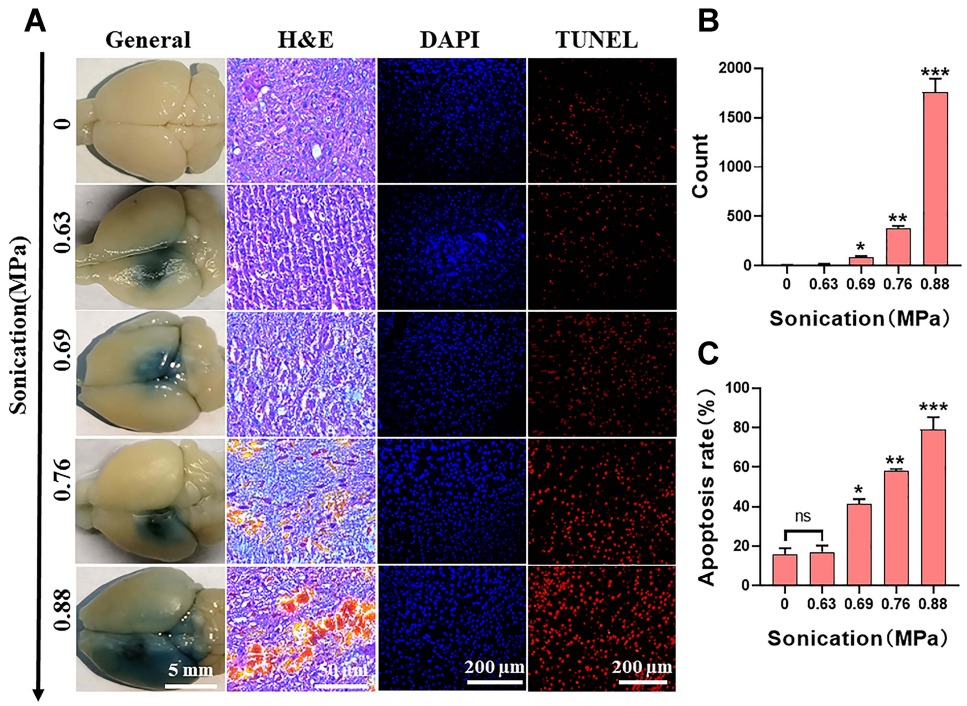

Figure 9 It is the most suitable and safe to open the ultrasonic parameters of BBB. (**A**) After the treatment of FUS with different sound pressure intensity combined with GA/PLGA-CMBs, the corresponding brain tissue was embedded in paraffin, stained with H&E, labeled with nucleus by DAPI and labeled with apoptotic cells by TUNEL. (**B**) When the ultrasonic intensity is 0.69–0.88Mpa, the erythrocyte extravasation is obvious (*p<0.05, **p<0.01, ***p<0.001 versus control group). (**C**) The apoptosis rate of TUNEL labeled apoptotic cells was counted by ImageJ software. The apoptosis rate is proportional to the sound pressure intensity (*p<0.05, **p<0.01, ***p<0.001 versus control group).

signal from the tumors was detected with a living imaging system (Figure 10A and B) and indicated the presence of tumor cells. The corresponding fluorescence signal in mice treated with FUS and GA/PLGA was 181.00 ± 13.52, and that of mice treated with FUS and GA/PLGA-CMB was 70.8 ± 8.03 ($p<0.05$). On day 24, the corresponding fluorescence signals of mice treated with FUS and GA/PLGA and mice treated with FUS and GA/PLGA-CMB were 148.4 ± 8.26 and 36.00 ± 4.82, respectively (Figure 10C, $p < 0.05$).

Tumor proliferation and apoptosis were detected by immunohistochemistry. The positive expression of markers of proliferation and apoptosis was observed by microscopy (Figure 11A). The tumor proliferation rate of each group was detected with immunohistochemistry utilizing an anti-PCNA antibody, and the tumor proliferation rate in mice treated with FUS and GA/PLGA-CMB was 31.77 ± 3.57% ($p < 0.001$ vs control group; Figure 11B). In addition, the tumor proliferation rate of each group was detected by an anti-Ki-67 antibody, and the tumor tissue growth rate of mice treated with FUS and GA/PLGA-CMB was 25.94 ± 3.12% ($p<0.001$ vs control group; Figure 11C). A TUNEL antibody was used to detect apoptosis within the tumors of each group of similarly treated mice. The results showed that the rate of apoptosis of tumor tissue in mice treated with FUS and GA/PLGA-CMB group was 78.98 ± 7.15% ($p<0.001$ vs control group; Figure 11D).

Mice were also subjected to general tests for anti-tumor viability following the treatment. On the 37th day after the establishment of the model, the brains of the mice in each treatment group were perfused for observation (Figure 12A). The volume of tumors from mice treated with FUS and GA/PLGA was 0.17 ± 0.04 mm^3, while the volume of tumors from mice treated with FUS and GA/PLGA-CMB was 0.04 ± 0.01 mm^3 ($p<0.001$ vs control group; Figure 12B). This reduction in tumor size correlated with life span, as the longest lived mice were those treated with FUS and GA/PLGA-CMB group, which lived 45±11 d ($p<0.05$ versus GA/PLGA group; Figure 12C).

Discussion

Delivering chemotherapeutic drugs into brain tumors remains an important challenge.[30] The existence of biological barriers such as the BBB and BTB limits the penetration of most chemotherapeutic agents.[8] In addition, the complexity

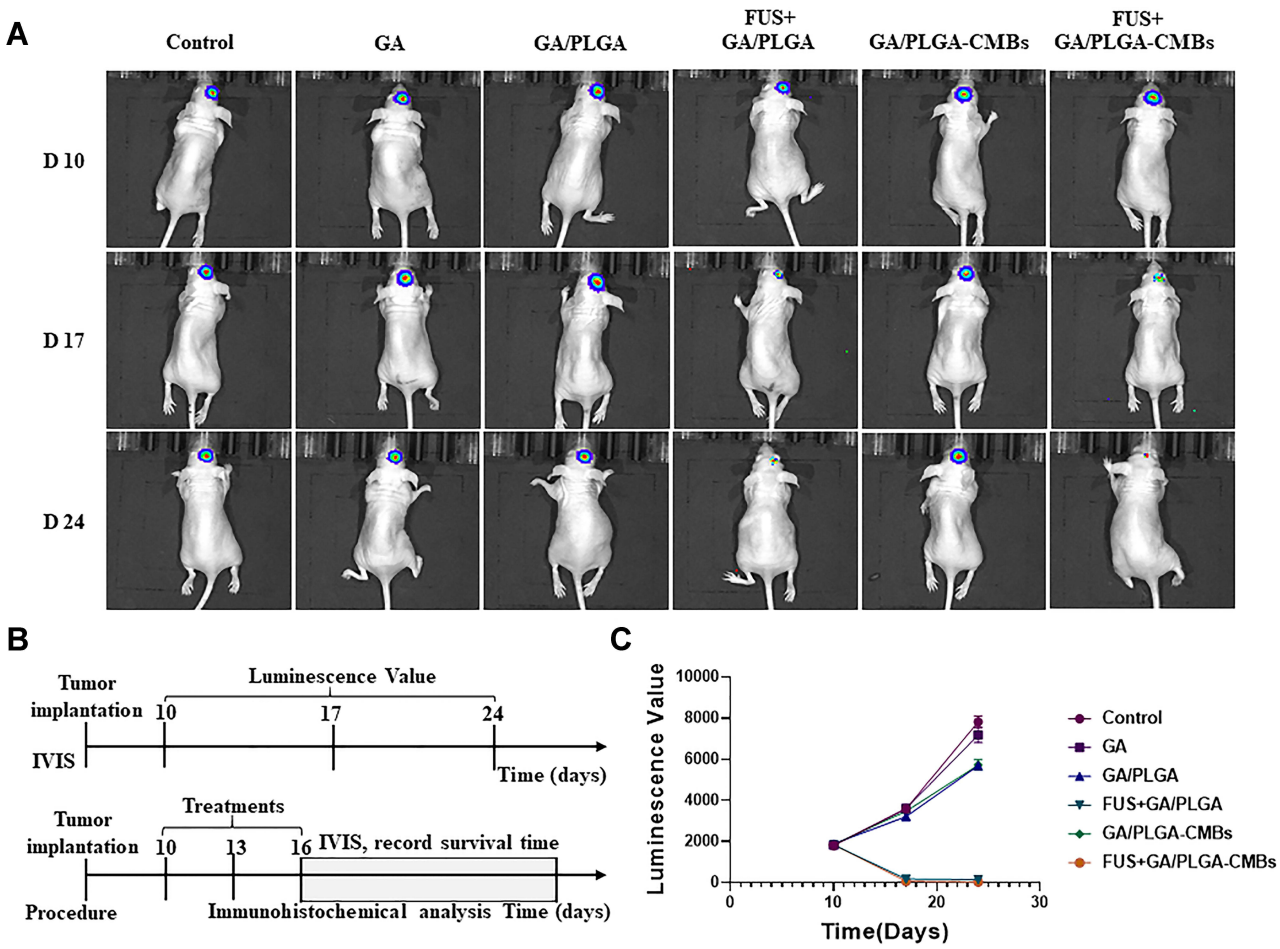

Figure 10 The anti-tumor effect was evaluated by in vivo imaging system (IVIS). (**A** and **B**) U87 cells carrying GFP-Luc-Puro gene fragments were selected for modeling. The glioma model mice were treated on the 10th day, once/2 days, for 3 times. The mice in each group were detected by IVIS on the 10th day, 17th day and 24th day, respectively. (**C**) The fluorescence signal values of mice in different treatment groups. The corresponding fluorescence signal curves of FUS+GA/PLGA-CMBs group and FUS+GA/PLGA group were lower.

of brain tumors and the lack of effective brain drug delivery techniques have had a significant impact on the survival of patients. Among different types of brain tumors, GBM is a highly invasive, aggressive and malignant tumor. New treatments for this important disease are needed. Recent studies have shown that ultrasound targeted microbubble destruction (UTMD) can safely and effectively open the BBB and BTB and deliver drugs to brain tissue, which provides a new strategy for the treatment of brain diseases.[19,23,24,31,32]

Because of the potential advantages of the UTMD system, we developed a new drug-loaded microbubble complex (PLGA-CMB) using DSPC, PEG-2000, PEI and PLGA as raw materials. PLGA-CMB was found to be stable, to have a high drug loading content, and to provide a long imaging duration in vivo. To take advantage of these properties, we prepared PLGA-CMB complexes containing GA (Figure 1).

PLGA-CMB complexes consist of drug-loaded PLGA nano-microbubbles and phospholipid cationic microbubbles, and in particular, our previous studies have shown that drug-loaded PLGA nano-microbubbles have good stability.[33] In addition, the core of phospholipid cationic microbubbles is an inert gas (C_3F_8) that has been shown to be relatively stable under physiological condition.[34–37] The results of Omata et al, who found that perfluoropropane and perfluorobutane-loaded MBs (MB-C_3F_8 and MB-C_4F_{10}) showed sustained ultrasound imaging stability in vitro and in vivo compared with sulfur hexafluoride-loaded MBs (MB-SF_6),[37] suggested that perfluoropropane and perfluorobutane could be useful for the production of MBs with high stability to allow for US imaging and drug delivery.[37] In this study, the

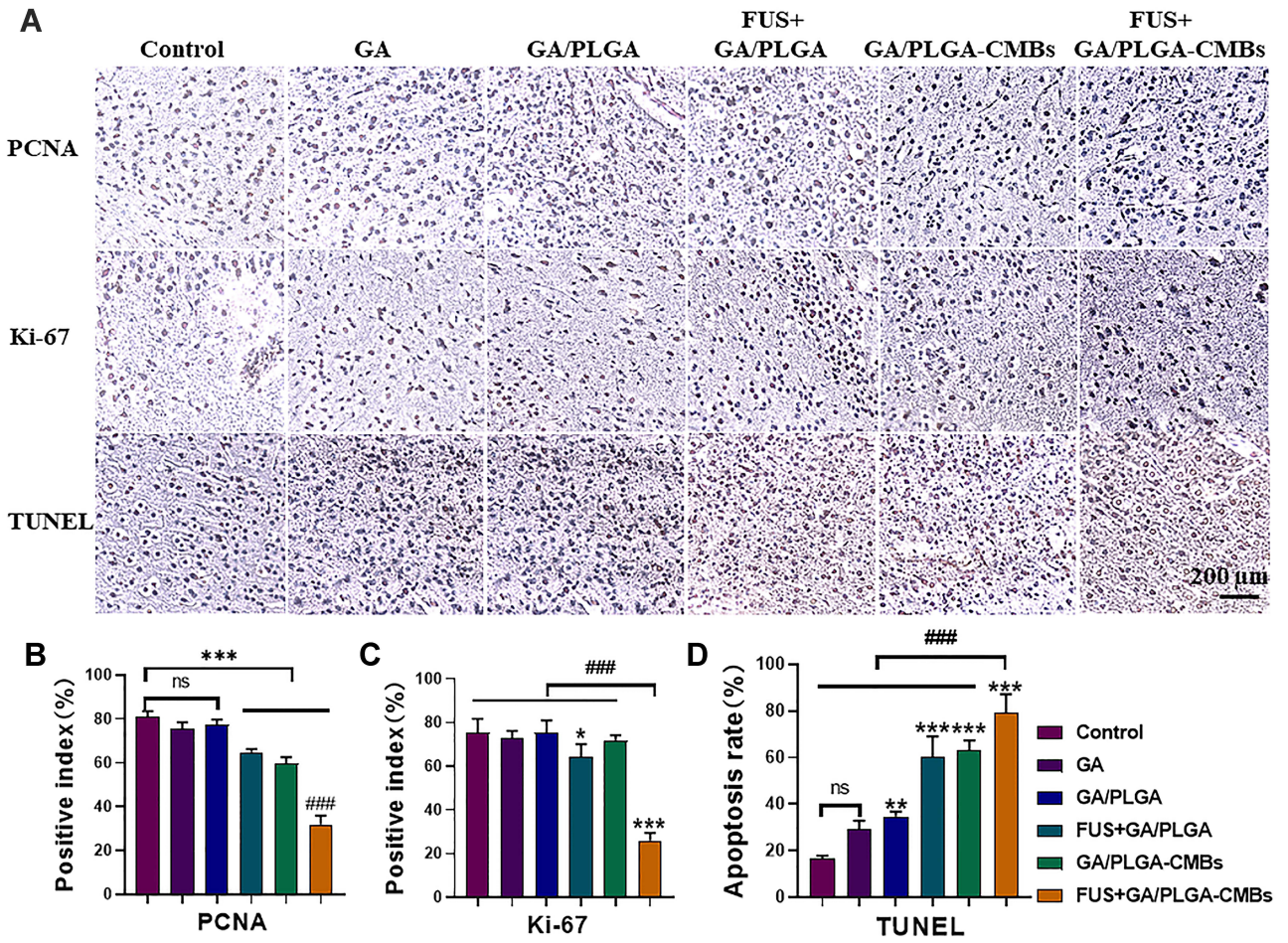

Figure 11 The anti-tumor effect was evaluated by immunohistochemistry. (**A**–**D**) On the 17th day of modeling, the brains of mice in different treatment groups were perfused and the corresponding tumor tissues were sectioned in paraffin. Tumor proliferation was detected by PCNA antibody and Ki-67 antibody, and tumor apoptosis was detected by TUNEL antibody (*p<0.05, **p<0.01, ***p<0.001 versus control group, ###p<0.001 versus each other group).

results shows that PLGA-CMB complexes, with C_3F_8 core, have optimal stability under physiological conditions (Figure 6).

Our previous studies have shown that porous lipid GA/PLGA microbubbles combined with FUS have led to an opening of an in vitro BBB model.[33] However, we found that the opening effect of porous lipid GA/PLGA microbubbles combined with FUS on the BBB in vivo is not ideal. Therefore, here, we developed a new type of GA/PLGA-CMBs complex that incorporates microbubble technology. Compared with GA/PLGA, GA/PLGA-CMBs have a more obvious opening effect on the BBB in vivo under the action of FUS.

In this study, PLGA nanoparticles containing GA were prepared by the double emulsion method.[38,39] Negatively charged GA/PLGA nanoparticles were connected to the surface of positively charged cationic microbubbles (CMBs) to form GA/PLGA-CMB microbubble complexes.[34,40] We demonstrate that GA/PLGA-CMBs can produce a sound pore effect under the action of FUS, which leads to the increase of cell membrane permeability.[41] In in vitro experiments, the cavitation effect supported by GA/PLGA-CMB under the action of low frequency FUS induced permeability of the cell membrane, which further improved the killing effect of GA on two GBM cell lines, U87 and U251.[42,43]

When a suspension containing GA/PLGA-CMB was injected into the caudal vein of mice, it ultimately reached the area of the induced brain tumor via the circulation. Under the action of FUS with specific sound pressure intensities, steady-state cavitation occurred in the GA/PLGA-CMB complexes, resulting in an increase in the permeability of the BBB and BBTB. GA/PLGA-CMB was uniformly distributed in the tumor tissue area, which resulted in increased sound

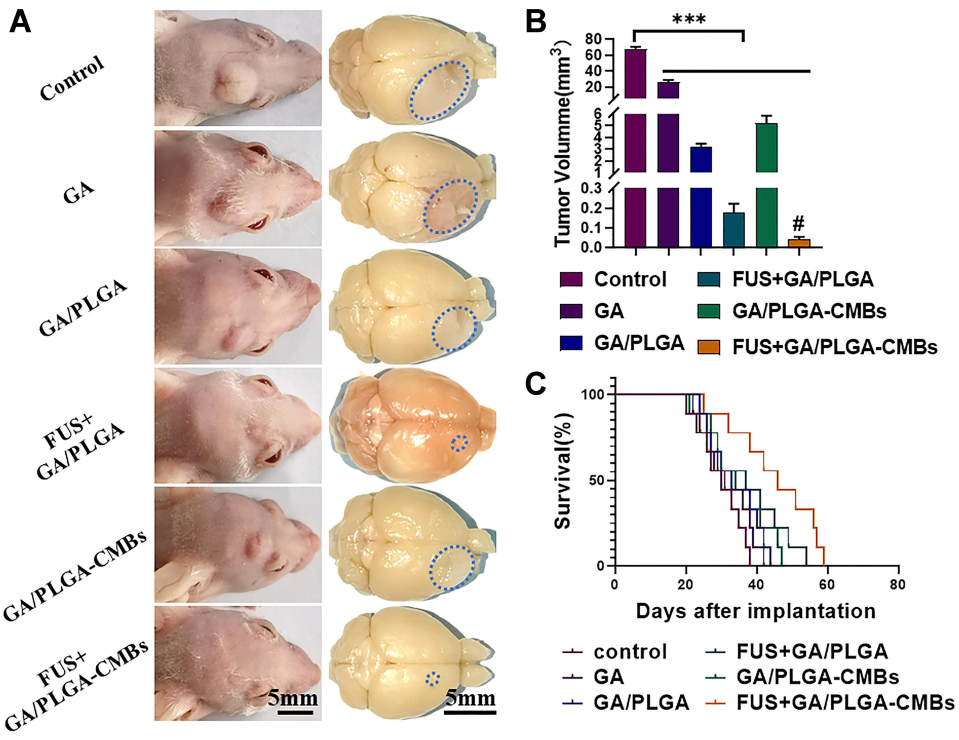

Figure 12 The anti-tumor effect was evaluated by general index. (**A**) After 37 days of modeling, the mice in different treatment groups corresponded to the gross view of glioma. (**B**) Quantification of tumor volume in mice with different treatment groups (***p<0.001 versus control group, #p<0.05 versus each other group). (**C**) The survival rate of six groups of mice was counted. The life cycle of mice in FUS+GA/PLGA-CMBs group was the longest, which was 59 days.

pressure intensity, causing instantaneous cavitation of the GA/PLGA-CMB, destroying the tumor tissue and releasing GA/PLGA to the tumor area. Thus, we have demonstrated a means to provide targeted treatment of brain tumors. It is important to note that PLGA has good biocompatibility and improves the efficiency of GA. Overall, our experimental results show that application of GA/PLGA-CMB combined with FUS has positive anti-tumor effects.

Notably, these results suggest that these efforts may be expanded to the visual targeting of anti-tumor therapies. Visual targeting makes use of ultrasonic imaging, which is a real-time imaging technology that can visualize the structures of organs.[44–46] MBs in particular can be used as contrast agents to enhance the utility of ultrasound images.[45] By choosing the appropriate ultrasound frequency and other ultrasound parameters, we predict that it will be possible to realize tumor imaging and tracking of the drug release process of GA/PLGA-CMBs under the action of FUS. In addition, this technique will allow the detection of the viability of microbubbles in vivo through passive cavitation detection, which has been tested widely in clinical trials.[28,47,48]

The ultrasonic parameters such as sound pressure intensity, duty cycle, action time, cycle time and pulse interval have obvious influences on the effects of FUS. Our results show that when other parameters are constant and microbubbles are combined with ultrasound, as the sound pressure intensity increases, the cavitation effect becomes more obvious, and the permeability of the physiological barrier becomes higher. For our next step, then, we plan to use this method to carry out in vivo experimental research to explore the safety range of FUS parameters. Whether the shell will cause inflammation after the rupture of microbubbles will also be a focus of attention. The biosafety of microbubbles is also of great concern, and we plan to systematically evaluate the biosafety of GA/PLGA-CMB.[28,49,50]

Conclusion

We have developed a new type of drug-loaded microbubble complex (PLGA-CMB). The microbubble complex can carry drugs with high volume. PLGA-CMBs can produce a cavitation effect under the action of UTMD and can thus open up the BBB and BBTB to efficiently target brain tumors. This microbubble complex provides a new strategy for the

ultrasound-targeted treatment of tumors. Effective on-demand drug delivery can be achieved by using PLGA-CMBs in a sonodynamic-dependent manner both in vitro and in vivo. The explosion of PLGA-CMBs under the action of FUS provides a promising platform for the delivery of anti-tumor therapeutic agents.

Acknowledgments

The study was supported by the grant from National Key R&D Program of China (2020YFA0908800), the National Natural Science Fund of China (grant no. U1804187, 81971638, 12074269), Shenzhen Science and Technology Program (JCYJ20210324105415040, JCYJ20190809105207439) and Guangdong Natural Science Fund (2020A1515010395).

Disclosure

The authors report no conflicts of interest in this work.

References

1. Wirsching HG, Galanis E, Weller M. Glioblastoma. *Handb Clin Neurol*. 2016;134:381–397. doi:10.1016/B978-0-12-802997-8.00023-2
2. Le Rhun E, Preusser M, Roth P, et al. Molecular targeted therapy of glioblastoma. *Cancer Treat Rev*. 2019;80:101896. doi:10.1016/j.ctrv.2019.101896
3. Tejada Solís S, Plans Ahicart G, Iglesias Lozano I, et al. Glioblastoma treatment guidelines: consensus by the Spanish society of neurosurgery tumor section. *Neurocirugia*. 2020;31(6):289–298. doi:10.1016/j.neucir.2020.06.001
4. Treder M, Janssen S, Holländer NH, Schild SE, Rades D. Role of neoadjuvant radio-chemotherapy for the treatment of high rectal cancer. *Anticancer Res*. 2018;38(9):5371–5377. doi:10.21873/anticanres.12866
5. van den Ende T, van den Boorn HG, Hoonhout NM, et al. Priming the tumor immune microenvironment with chemo(radio)therapy: a systematic review across tumor types. *Biochim Biophys Acta Rev Cancer*. 2020;1874(1):188386. doi:10.1016/j.bbcan.2020.188386
6. Rawal S, Patel MM. Threatening cancer with nanoparticle aided combination oncotherapy. *J Control Release*. 2019;301:76–109. doi:10.1016/j.jconrel.2019.03.015
7. Anselmo AC, Mitragotri S. Nanoparticles in the clinic: an update. *Bioeng Transl Med*. 2019;4(3):e10143. doi:10.1002/btm2.10143
8. Janjua TI, Rewatkar P, Ahmed-Cox A, et al. Frontiers in the treatment of glioblastoma: past, present and emerging. *Adv Drug Deliv Rev*. 2021;171:108–138. doi:10.1016/j.addr.2021.01.012
9. Bonvalot S, Rutkowski PL, Thariat J, et al. NBTXR3, a first-in-class radioenhancer hafnium oxide nanoparticle, plus radiotherapy versus radiotherapy alone in patients with locally advanced soft-tissue sarcoma (Act.In.Sarc): a multicentre, Phase 2–3, randomised, controlled trial. *Lancet Oncol*. 2019;20(8):1148–1159. doi:10.1016/S1470-2045(19)30326-2
10. Kang JH, Cho J, Ko YT. Investigation on the effect of nanoparticle size on the blood-brain tumour barrier permeability by in situ perfusion via internal carotid artery in mice. *J Drug Target*. 2019;27(1):103–110. doi:10.1080/1061186X.2018.1497037
11. Mo J, He L, Ma B, Chen T. Tailoring particle size of mesoporous silica nanosystem to antagonize glioblastoma and overcome blood–brain barrier. *ACS Appl Mater Interfaces*. 2016;8(11):6811–6825. doi:10.1021/acsami.5b11730
12. Guillet-Nicolas R, Popat A, Bridot JL, Monteith G, Qiao SZ, Kleitz F. pH-responsive nutraceutical-mesoporous silica nanoconjugates with enhanced colloidal stability. *Angew Chem Int Ed Engl*. 2013;52(8):2318–2322. doi:10.1002/anie.201208840
13. Um W, Park J, Youn A, et al. A comparative study on albumin-binding molecules for targeted tumor delivery through covalent and noncovalent approach. *Bioconjug Chem*. 2019;30(12):3107–3118. doi:10.1021/acs.bioconjchem.9b00760
14. Liu Y, Chen Y, Lin L, Li H. Gambogic acid as a candidate for cancer therapy: a review. *Int J Nanomedicine*. 2020;15:10385–10399. doi:10.2147/IJN.S277645
15. Hatami E, Jaggi M, Chauhan SC, Yallapu MM. Gambogic acid: a shining natural compound to nanomedicine for cancer therapeutics. *Biochim Biophys Acta Rev Cancer*. 2020;1874(1):188381. doi:10.1016/j.bbcan.2020.188381
16. Pandey MK, Karelia D, Amin SG. Gambogic acid and its role in chronic diseases. *Adv Exp Med Biol*. 2016;928:375–395. doi:10.1007/978-3-319-41334-1_15
17. Tang X, Liu C, Li T, et al. Gambogic acid alleviates inflammation and apoptosis and protects the blood-milk barrier in mastitis induced by LPS. *Int Immunopharmacol*. 2020;86:106697. doi:10.1016/j.intimp.2020.106697
18. Chen J, Li L, Zhou Y, Zhang J, Chen L. Gambogic acid ameliorates high glucose- and palmitic acid-induced inflammatory response in ARPE-19 cells via activating Nrf2 signaling pathway: ex vivo. *Cell Stress Chaperones*. 2021;26(2):367–375. doi:10.1007/s12192-020-01182-1
19. Shi D, Guo L, Sun X, et al. UTMD inhibit EMT of breast cancer through the ROS/miR-200c/ZEB1 axis. *Sci Rep*. 2020;10(1):6657. doi:10.1038/s41598-020-63653-w
20. Qu F, Wang P, Zhang K, et al. Manipulation of mitophagy by "All-in-One" nanosensitizer augments sonodynamic glioma therapy. *Autophagy*. 2020;16(8):1413–1435. doi:10.1080/15548627.2019.1687210
21. Wu QL, Xu HL, Xiong C, et al. c(RGDyk)-modified nanoparticles encapsulating quantum dots as a stable fluorescence probe for imaging-guided surgical resection of glioma under the auxiliary UTMD. *Artif Cells Nanomed Biotechnol*. 2020;48(1):143–158. doi:10.1080/21691401.2019.1699821
22. Li Y, Du M, Fang J, Zhou J, Chen Z. UTMD promoted local delivery of miR-34a-mimic for ovarian cancer therapy. *Drug Deliv*. 2021;28(1):1616–1625. doi:10.1080/10717544.2021.1955041
23. Liao Y, Luo H, He Z, et al. A combination of UTMD-mediated HIF-1α shRNA transfection and TAE in the treatment of hepatic cancer. *Biomed Res Int*. 2019;2019:1937460. doi:10.1155/2019/1937460
24. Ye L, Zhu X, He Y, Wei X. Ultrasonic cavitation damage characteristics of materials and a prediction model of cavitation impact load based on size effect. *Ultrason Sonochem*. 2020;66:105115. doi:10.1016/j.ultsonch.2020.105115

25. Datar S, Cabanillas M, Dadu R, Ost D, Grosu HB. Pulmonary cavitation in patients with thyroid cancer receiving antiangiogenic agents. *BMC Cancer*. 2020;20(1):1181. doi:10.1186/s12885-020-07693-5
26. Hu M, Wang F, Huo P, et al. Nanoparticle-mediated cavitation via CO(2) laser impacting on water: concentration effect, temperature visualization, and core-shell structures. *Sci Rep*. 2019;9(1):18326. doi:10.1038/s41598-019-54531-1
27. Liu C, Li X, Li A, Cui Z, Chen L, Li Y. Cavitation onset caused by a dynamic pressure wave in liquid pipelines. *Ultrason Sonochem*. 2020;68:105225. doi:10.1016/j.ultsonch.2020.105225
28. Xu T, Cui Z, Li D, et al. Cavitation characteristics of flowing low and high boiling-point perfluorocarbon phase-shift nanodroplets during focused ultrasound exposures. *Ultrason Sonochem*. 2020;65:105060. doi:10.1016/j.ultsonch.2020.105060
29. Harzali H, Baillon F, Louisnard O, Espitalier F, Mgaidi A. Experimental study of sono-crystallisation of ZnSO4·7H2O, and interpretation by the segregation theory. *Ultrason Sonochem*. 2011;18(5):1097–1106. doi:10.1016/j.ultsonch.2011.03.007
30. Arvanitis CD, Ferraro GB, Jain RK. The blood-brain barrier and blood-tumour barrier in brain tumours and metastases. *Nat Rev Cancer*. 2020;20(1):26–41. doi:10.1038/s41568-019-0205-x
31. Lin L, Fan Y, Gao F, et al. UTMD-promoted co-delivery of gemcitabine and miR-21 inhibitor by dendrimer-entrapped gold nanoparticles for pancreatic cancer therapy. *Theranostics*. 2018;8(7):1923–1939. doi:10.7150/thno.22834
32. Wang Z, Jiang S, Li S, et al. Targeted galectin-7 inhibition with ultrasound microbubble targeted gene therapy as a sole therapy to prevent acute rejection following heart transplantation in a Rodent model. *Biomaterials*. 2020;263:120366. doi:10.1016/j.biomaterials.2020.120366
33. Wang F, Dong L, Wei X, et al. Effect of gambogic acid-loaded porous-Lipid/PLGA microbubbles in combination with ultrasound-triggered microbubble destruction on human glioma. *Front Bioeng Biotechnol*. 2021;9:711787. doi:10.3389/fbioe.2021.711787
34. Manta S, Renault G, Delalande A, et al. Cationic microbubbles and antibiotic-free miniplasmid for sustained ultrasound-mediated transgene expression in liver. *J Control Release*. 2017;262:170–181. doi:10.1016/j.jconrel.2017.07.015
35. Shan L Perfluoropropane-filled, sorbitan monostearate– and polyoxyethylene 40 stearate–shelled nanobubbles. Bethesda (MD).2004.
36. Schutt EG, Klein DH, Mattrey RM, Riess JG. Injectable microbubbles as contrast agents for diagnostic ultrasound imaging: the key role of perfluorochemicals. *Angew Chem Int Ed Engl*. 2003;42(28):3218–3235. doi:10.1002/anie.200200550
37. Omata D, Maruyama T, Unga J, et al. Effects of encapsulated gas on stability of lipid-based microbubbles and ultrasound-triggered drug delivery. *J Control Release*. 2019;311–312:65–73. doi:10.1016/j.jconrel.2019.08.023
38. Pagano A, Khalid N, Kobayashi I, Nakajima M, Neves MA, Bastos EL. Microencapsulation of betanin in monodisperse W/O/W emulsions. *Food Res Int*. 2018;109:489–496. doi:10.1016/j.foodres.2018.04.053
39. Liu J, Kharat M, Tan Y, Zhou H, Muriel Mundo JL, McClements DJ. Impact of fat crystallization on the resistance of W/O/W emulsions to osmotic stress: potential for temperature-triggered release. *Food Res Int*. 2020;134:109273. doi:10.1016/j.foodres.2020.109273
40. Delalande A, Bastié C, Pigeon L, et al. Cationic gas-filled microbubbles for ultrasound-based nucleic acids delivery. *Biosci Rep*. 2017;37(6):6. doi:10.1042/BSR20160619
41. Aghajanpoor M, Hashemi-Najafabadi S, Baghaban-Eslaminejad M, Bagheri F, Mohammad Mousavi S, Azam Sayyahpour F. The effect of increasing the pore size of nanofibrous scaffolds on the osteogenic cell culture using a combination of sacrificial agent electrospinning and ultrasonication. *J Biomed Mater Res A*. 2017;105(7):1887–1899. doi:10.1002/jbm.a.36052
42. Karthikesh MS, Yang X. The effect of ultrasound cavitation on endothelial cells. *Exp Biol Med (Maywood)*. 2021;246(7):758–770. doi:10.1177/1535370220982301
43. Zheng J, Guo Y, Zhu L, Deng H, Shang Y. Cavitation effect in two-dimensional ultrasonic rolling process. *Ultrasonics*. 2021;115:106456. doi:10.1016/j.ultras.2021.106456
44. Chen R, Jiang L, Zhang T, et al. Eco-friendly highly sensitive transducers based on a new KNN-NTK-FM lead-free piezoelectric ceramic for High-Frequency biomedical ultrasonic imaging applications. *IEEE Trans Biomed Eng*. 2019;66(6):1580–1587. doi:10.1109/TBME.2018.2876063
45. Wells PN, Liang HD, Young TP. Ultrasonic imaging technologies in perspective. *J Med Eng Technol*. 2011;35(6–7):289–299. doi:10.3109/03091902.2011.595531
46. Wischhusen J, Wilson KE, Delcros JG, et al. Ultrasound molecular imaging as a non-invasive companion diagnostic for netrin-1 interference therapy in breast cancer. *Theranostics*. 2018;8(18):5126–5142. doi:10.7150/thno.27221
47. Haworth KJ, Bader KB, Rich KT, Holland CK, Mast TD. Quantitative frequency-domain passive cavitation imaging. *IEEE Trans Ultrason Ferroelectr Freq Control*. 2017;64(1):177–191. doi:10.1109/TUFFC.2016.2620492
48. Li T, Chen H, Khokhlova T, et al. Passive cavitation detection during pulsed HIFU exposures of ex vivo tissues and in vivo mouse pancreatic tumors. *Ultrasound Med Biol*. 2014;40(7):1523–1534. doi:10.1016/j.ultrasmedbio.2014.01.007
49. Cheng M, Li F, Han T, Yu A, Qin P. Effects of ultrasound pulse parameters on cavitation properties of flowing microbubbles under physiologically relevant conditions. *Ultrason Sonochem*. 2019;52:512–521. doi:10.1016/j.ultsonch.2018.12.031
50. Yao Y, Xiao H, Zhu L, et al. Ultrasound-mediated oxygen delivery for enhanced radiotherapy with ultrasound imaging guidance. *J Biomed Nanotechnol*. 2020;16(11):1633–1643. doi:10.1166/jbn.2020.2990